JOURNAL OF CATALYSIS 151, 266–278 (1995)

Dynamic and LHHW Kinetic Analysis of Heterogeneous Catalytic Hydroformylation

Michael W. Balakos and Steven S. C. Chuang[1]

Department of Chemical Engineering, The University of Akron, Akron, Ohio 44325-3906

Received May 2, 1994; revised September 8, 1994

Heterogeneous ethylene hydroformylation on a 4 wt% Rh/SiO_2 catalyst was studied using a steady-state pulse transient method coupled with *in situ* infrared spectroscopy. Four independent quantities, including the rates of propionaldehyde and ethane formation and the surface coverages of adsorbed CO and adsorbed acyl species, were measured at steady state as a function of the partial pressures of the reactants. The coverage of intermediates during ethylene hydroformylation was determined from the dynamic response of $C_2H_5{}^{13}CHO$ to a ^{13}CO pulse input. The coverage of adsorbed CO was measured by *in situ* IR spectroscopy. The rate laws for C_2H_5CHO and C_2H_6 formation and the isotherm equations for adsorbed C_2H_5CO and adsorbed CO were derived using the Langmuir–Hinshelwood–Hougen–Watson (LHHW) approach from a proposed mechanism with the hydrogenation of adsorbed C_2H_5CO as the rate-determining step for propionaldehyde formation and the hydrogenation of adsorbed C_2H_5 as the rate-determining step for ethane formation. The high degree of fitting of rate and coverage data to the derived rate law and isotherm equations suggests that the LHHW model describes the surface reaction with high accuracy. Although the assumptions for the Langmuir isotherm do not account for the interactions between adsorbates, the LHHW equations and the proposed mechanism satisfactorily describe the kinetics, reaction pathways, and rate-limiting steps for the formation of ethane and propionaldehyde. This study demonstrates that the measurement of coverage of adsorbates by isotopic tracer pulsing and *in situ* infrared spectroscopy provides direct experimental evidence to confirm a postulated mechanism and rate law.

INTRODUCTION

The determination of reliable rate expressions is paramount in the design and modeling of heterogeneously catalyzed processes. The kinetics of heterogeneous catalytic reactions has been studied for many years (1–5). Hougen and Watson (1, 6) first extended the Langmuir theory of adsorption and applied it to the rates of catalytic reactions. Tschernitz *et al.* (7) applied the approach to the hydrogenation of mixed iso-octenes (the "codimer" example). The type of rate equations derived from this approach are now commonly called Langmuir–Hinshelwood–Hougen–Watson (LHHW) kinetics (8–10).

Despite the wide use of LHHW kinetics, the formalism has been the subject of much discussion and criticism. First, the heat of adsorption for many adsorbate–adsorbent systems varies with the surface coverage of the adsorbate (5). As a result, not all adsorption isotherms of a single reactant can be represented by a Langmuir isotherm because it does not account for interactions between adsorbates. It is therefore doubtful that the behavior of an adsorbate in multicomponent systems would follow a Langmuir isotherm under reaction conditions. However, the LHHW equation derived from the Langmuir isotherm often provides a good fit of the rate data (8). Other types of isotherms accounting for the variation of heat of adsorption with coverage have been applied to kinetic studies and were found to fit experimental data with an equal amount of accuracy (11). Indeed, it is not difficult to obtain a good fit of the rate data to rate expressions with a number of adjustable parameters, usually more than three. Second, the postulation of a different mechanism or rate-determining step may lead to the same form of rate equations in the LHHW kinetic framework (12, 13). Third, the adsorption constants found by fitting the LHHW equations to experimental data are rarely equal to adsorption constants measured from chemisorption experiments (3, 5). These criticisms led to the opinion that the LHHW formalism is nothing more than a systematic data fitting technique (14–16). Most of the criticisms in the LHHW formalism are the result of the inability to measure the coverage of adsorbates and reaction intermediates as a function of partial pressure of reactants and the inability to identify the rate-determining step *during* the reaction (17, 18). An alternative is empirical power-law rate expressions that have wide applicability, provide a straight forward relationship between rate and partial pressure of reactant, and are easy to fit to experimental data with conventional techniques (14, 17). It has also been pointed out that power-law rate expressions have a theoretical

[1] To whom all correspondence should be addressed.

0021-9517/95 $6.00

basis when nonuniform surfaces are taken into consideration (15).

It has been suggested that LHHW kinetics provides insight into the mechanism of the reaction and may lead to a fundamental understanding of the reaction (19). Boudart suggested that LHHW kinetics is not only useful, but also correct for structure-insensitive reactions (20, 21). Structure-insensitive reactions are those for which the rate of reaction is independent of the particle size or surface structure of the catalyst crystallites. Structure-insensitivity has been observed for catalytic reactions taking place under high surface coverage of adsorbates (20). It has been postulated that the effects of surface nonuniformities may be insignificant compared to surface interactions under high surface coverage (20). Many catalytic reactions which have been termed structure-insensitive have been described successfully by LHHW kinetics (4). Adsorption parameters estimated for hydrogenation reactions, which are generally structure-insensitive, have been found to be consistent with thermodynamic constraints (22, 23).

Heterogeneous olefin hydroformylation, the reaction of an olefin with syngas to form an aldehyde, has been found to be structure-insensitive and can be described by LHHW kinetics (24–28). The main products from heterogeneous ethylene hydroformylation are propionaldehyde (the product of hydroformylation), and ethane (the product of ethylene hydrogenation). Hydroformylation is the largest industrial homogeneously catalyzed reaction with a selectivity of greater than 98% toward the aldehyde product. Due to high costs of separating the homogeneous catalyst from the products, much effort has been directed toward the development of a heterogeneous catalyst. The reaction of ethylene with syngas has also been used as a probe reaction to study the activity and selectivity in the Fischer–Tropsch process on supported transition metals (29–32). The objectives of this investigation are to combine isotopic transient and *in situ* IR methods to study heterogeneous hydroformylation and to test a LHHW model that can describe the overall kinetics and is consistent with the adsorption isotherms of surface intermediates. Heterogeneous ethylene hydroformylation on a 4 wt% Rh/SiO_2 catalyst is used as a model reaction for this purpose. Kinetic equations will be derived from the LHHW formalism and the postulation of a rate-determining step for both propionaldehyde and ethane formation. *In situ* infrared (IR) coupled with transient isotopic tracing will be used to measure the coverage of adsorbed species during the reaction and to compare it to the coverage predicted by the LHHW method.

EXPERIMENTAL

Catalyst Preparation and Characterization

A 4 wt% Rh/SiO_2 catalyst was prepared by the incipient wetness impregnation method. An aqueous solution of $RhCl_3 \cdot 3H_2O$ (Alfa Products) was impregnated into a large pore SiO_2 support (Strem Chemicals, surface area of 350 m^2/g). The ratio of the volume of solution to the weight of silica support used in the impregnation step was 1 cm^3 to 1 g. After impregnation, the sample powder was dried in air at 298 K overnight and then reduced under flowing hydrogen at 673 K for 16 hr. The H_2 uptake of the catalyst was measured at 303 K by a pulse adsorption method and was found to be 122 μmol/g. This corresponds to a dispersion of 0.62 and a crystallite size of 15 Å, assuming an adsorption stoichiometry of $H_{ads}/Rh = 1$ and a cubic shape for the Rh crystallites.

Experimental Apparatus and Procedure

The apparatus used in this study is similar to that previously reported (33) and will be briefly discussed here. Steady-state flows of CO, ^{13}CO, H_2, C_2H_4, and He were controlled by mass flow controllers to an infrared reactor cell. The CO contains 2 vol% Ar for determining the effect of gas-phase holdup in the reactor and the gas transportation lines on the transient response of gaseous products. The CO line upstream from the reactor contains a Valco 6-port pulsing valve for pulsing an amount of ^{13}CO into the CO flow. All reactant gases are combined at a mixing point before the IR reactor cell.

The *in situ* infrared spectra were recorded by a Nicolet 5SXC spectrometer with a DTGS detector at a resolution of 4 cm^{-1}. The IR reactor cell, which can be operated up to 773 K and 6 MPa, acts as a differential reactor; therefore, the initial rates for the forward reaction can be obtained. Thirty-two scans were coadded when recording spectra under steady-state conditions, while only three scans were coadded under transient conditions to facilitate rapid scanning.

The transient responses of the gaseous products from the IR cell were recorded by a Balzers QMG112 mass spectrometer (MS) interfaced to a microcomputer. The MS is equipped with a differentially pumped inlet system located directly downstream of a pressure regulator for fast response time. The *m/e* ratios followed by the MS were 28 for CO, 29 for ^{13}CO, 40 for Ar, and 59 for $C_2H_5{}^{13}CHO$. The *m/e* ratios were carefully selected to prevent interference from the fragmentation of parent species. The concentrations of gaseous products were also analyzed by a HP-5890A gas chromatograph with an FID detector.

Approximately 60 mg of catalyst powder was pressed into three self-supporting disks. One disk was placed in the reactor directly in the pathway of the IR beam. To obtain accurate data, the other two disks were broken up and placed in the reactor against the outside rim of the disk and held in place with glass wool. The catalyst was further reduced under H_2 flow at 673 K and 0.1 MPa for

TABLE 1

Reaction Rate and Selectivity in Heterogeneous Hydroformylation on 4 wt% Rh/SiO_2 for $CO/H_2/C_2H_4/He$ = 1/1/1/1 and a Total Flowrate of 120 cm^3/min

Temperature (K)	Turnover frequency of product formation ($10^3 \cdot min^{-1}$)[a]						Selectivity[b]
	CH_4	C_2H_6	C_2H_5CHO	C_3H_6	C_4H_8	n-C_4H_{10}	
483	—	182	24.8	0.682	0.152	0.183	0.136
513	0.120	815	56.9	—	0.308	0.458	0.070
513	—	658	59.2	2.48	0.294	0.462	0.090
543	0.358	2020	122	8.93	15.4	28.8	0.060
573	29.5	5920	229	61.5	89.7	183	0.039

[a] The TOF values reported in this table are multiplied by 10^3.
[b] Selectivity is defined as $TOF_{C_2H_5CHO}/TOF_{C_2H_6}$.

2 h prior to the experiments. The reactant gas of $CO/H_2/C_2H_4/He$ was passed over the catalyst at a desired ratio and a total flowrate of 120 cm^3/min. Helium was used as a diluent for maintaining constant total flow rate while varying the partial pressures of the individual reactants. The products were monitored by the MS. After the reaction settled to steady state (approximately 5–10 min), a 10 cm^3 pulse of ^{13}CO into the CO stream was made, and the pulse transient response of adsorbed CO was recorded by the IR spectrometer and the gaseous products by the MS. It was attempted to keep the pressure within the sampling loop of the 6-port pulsing valve and that of the reactor exactly the same so as to maintain the steady-state of the reaction during the pulse injection of ^{13}CO. After each transient experiment, a bracketing technique (34) was used whereby the catalyst was heated under a H_2 atmosphere to 573 K for 10 min, held at 573 K for 10 min, and was cooled to the reaction temperature for 10 min to start the next experiment. This technique prevented deactivation and yielded good reproducibility as determined by repeating the experimental conditions at equal partial pressures of the reactants after all other experiments were run.

RESULTS

Steady-State Measurements

The steady-state rates of formation of ethane and propionaldehyde during heterogeneous hydroformylation on 4 wt% Rh/SiO_2 were measured by gas chromatography at 0.1 MPa. Table 1 lists the turnover frequencies (TOF) of all the hydrocarbon and oxygenate species detected in the temperature range 483–573 K and equal ratios of reactants and diluent ($CO/H_2/C_2H_4/He$ = 1/1/1/1). TOF is defined as the rate of product formation divided by the amount of surface exposed Rh metal atoms measured by H_2 chemisorption. The main products of the reaction are ethane and propionaldehyde. Other hydrocarbon products include methane, propylene, butene, and butane. The formation of methane from the Fischer–Tropsch synthesis has been previously reported to be suppressed by the presence of ethylene in the feed (32). The hydrocarbon products other than ethane and propionaldehyde make up 0.4% of the products at 483 K, and increase to 5.5% at 573 K. The selectivity for propionaldehyde formation, defined as the ratio of TOFs for ethane and propionaldehyde formation, decreases with increasing temperature. Figure 1 depicts an Arrhenius plot of ethane and propionaldehyde formation. From a fit of the Arrhenius equation, the activation energies are 13.7 and 21.1 kcal/mol for the formation of propionaldehyde and ethane, respectively. The measured activation energy for ethylene hydrogenation, $E_{C_2H_6}$, is higher than that previously reported for Ni

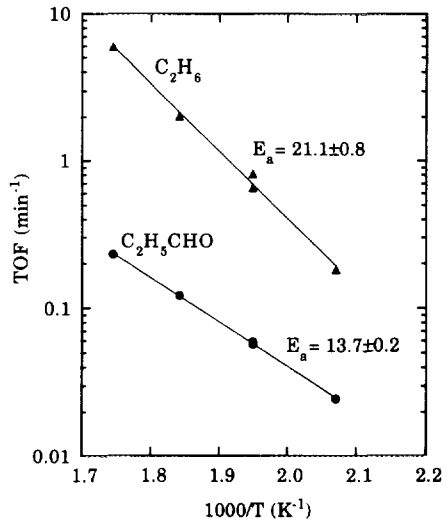

FIG. 1. Arrhenius plot of ethane and propionaldehyde formation on 4 wt% Rh/SiO_2 at 0.1 MPa and $CO/H_2/C_2H_4/He$ = 1/1/1/1.

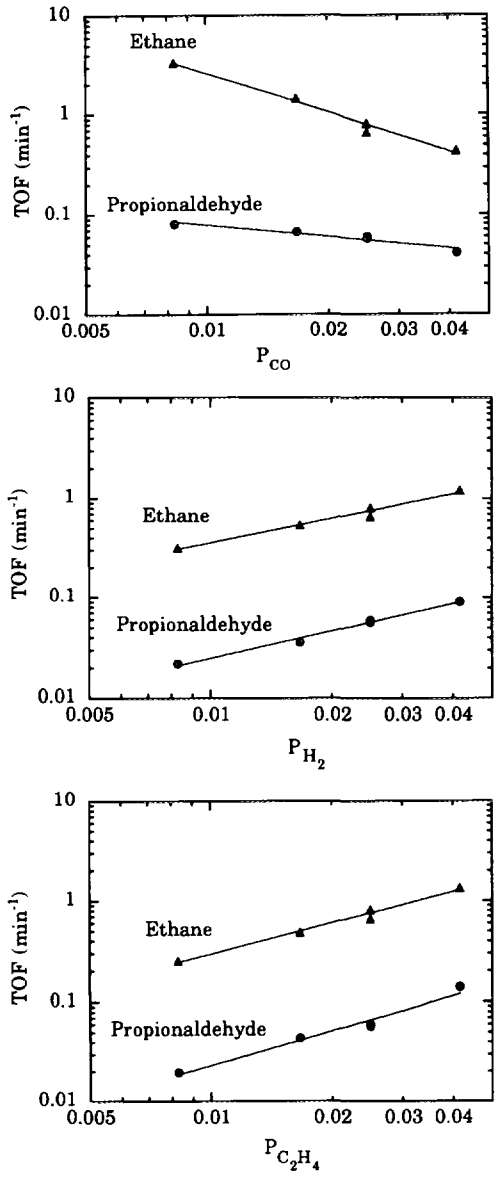

FIG. 2. The dependence of rate of ethane and propionaldehyde formation on the partial pressures of reactants at 513 K and a total pressure of 0.1 MPa.

film and supported Pt (35, 36) between 223 and 336 K; however, $E_{C_2H_6}$ agrees well with the results for olefin hydrogenation in hydroformylation on Rh/SiO_2 and zeolite-supported Rh (24, 27, 37). The higher activation energy in the presence of CO may be due to the inhibition of hydrogen and olefin adsorption brought about by adsorbed CO.

To determine the dependence of the reaction rates on the partial pressures of reactants, the rates were measured as the partial pressures were varied at a total pressure of 0.1 MPa and 513 K. The flowrate of He was varied to maintain a constant total flowrate of 120 cm^3/min. Figure 2 shows log–log plots of the TOF for ethane and propionaldehyde formation versus the partial pressures of CO, H_2, and C_2H_4. Both ethane and propionaldehyde formation rates are negative order in CO while positive order in both hydrogen and ethylene.

The *in situ* IR spectra during the experiments of varying partial pressures are shown in Figure 3. The top spectrum in Fig. 3 shows the variation of the spectra with CO partial pressure. The spectrum at a partial pressure of 0.0083 MPa exhibits a linear CO band at 2037 cm^{-1}; a small bridged CO band at 1885 cm^{-1}; a propionaldehyde band at 1740 cm^{-1}; and gaseous ethylene and ethane bands between 2900 and 3300 cm^{-1} (24, 25). The bridged CO band in this study is much smaller than a previous study in which the catalyst was reduced *in situ* at 503 K (24). The distinction between gaseous ethylene, ethane, and adsorbed hydrocarbon species is not possible due to strong overlapping. As the partial pressure of CO was increased, the wavenumber of the linear CO band increased to a final value of 2047 cm^{-1} at a partial pressure of 0.0417 MPa. The increase in wavenumber is due to an increase in dipole–dipole interaction resulting from increasing surface coverage of CO (38).

The other spectra in Fig. 3 show how the *in situ* IR spectra of ethylene hydroformylation reaction vary with the partial pressures of H_2 and C_2H_4, respectively. The IR spectra did not change while the partial pressure of

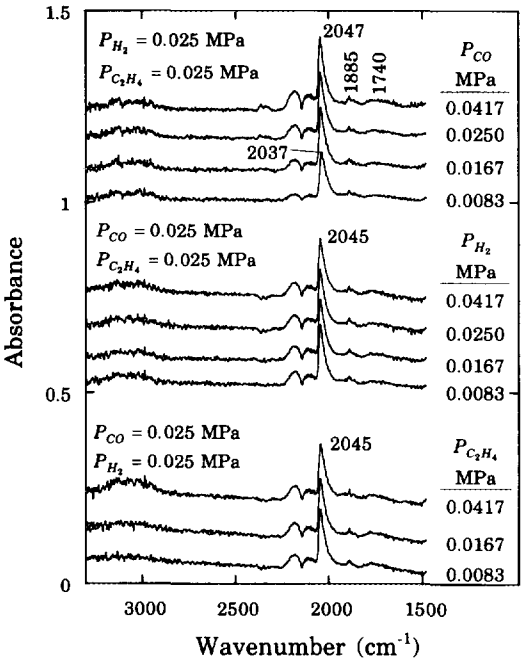

FIG. 3. *In situ* IR spectra of heterogeneous hydroformylation on 4 wt% Rh/SiO_2 at 0.1 MPa and 513 K at varying partial pressures of reactants.

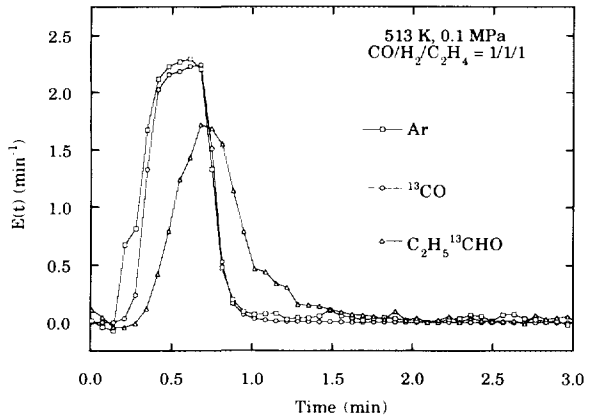

FIG. 4. The transient response of Ar, ^{13}CO, and $C_2H_5{}^{13}CHO$ to a pulse of ^{13}CO in the ^{12}CO feed during ethylene hydroformylation on 4 wt% Rh/SiO_2 at 513 K and 0.1 MPa.

H_2 increased from 0.0083 to 0.0417 MPa. The only change observed with varying ethylene partial pressure is an increase in the gaseous ethylene and ethane bands between 2800 and 3300 cm^{-1}. These results indicate that the surface coverage of adsorbed CO and propionaldehyde species is not a strong function of the partial pressures of hydrogen or ethylene in heterogeneous hydroformylation on Rh/SiO_2 at 0.1 MPa and 513 K.

Dynamic Measurements

The transient response of $C_2H_5{}^{13}CHO$ and the IR spectra to a 10-cm^3 pulse of ^{13}CO into the CO feed to the reactor were recorded during the steady-state experimental runs for which rate data are shown in Fig. 2. Figure 4 is the transient response of Ar, ^{13}CO, and $C_2H_5{}^{13}CHO$ measured by mass spectrometry under the conditions of 0.1 MPa, 513 K, and $CO/H_2/C_2H_4/He$ = 1/1/1/1. For comparison, the response is normalized to $E(t)$ and is defined as (8–10)

$$E(t) = \frac{C(t)}{\int_0^\infty C(t)dt}. \qquad [1]$$

It should be noted that the areas under all the normalized response curves are equal to 1. The time delay in the ^{13}C propionaldehyde response as compared to the Ar response curve is equivalent to the residence time of ^{13}C surface intermediates leading to ^{13}C propionaldehyde which is derived from ^{13}CO.

Figure 5a shows the IR spectra recorded during the isotopic pulse for which the MS response appears in Fig. 4. Figure 5a shows that gaseous ^{12}CO is replaced by ^{13}CO in the reactor for approximately 0.5 min, before returning to the original ^{12}CO flow. The linear ^{12}CO at 2045 cm^{-1} also exchanged with linear ^{13}CO at 1995 cm^{-1} at a rapid rate. Figure 5b presents the spectra recorded at time t and subtracted from the spectra before the switch and better represents the changes in adsorbates on the surface during the pulse. The gaseous ^{13}CO response in Fig. 4 corresponds to the exchange between linear CO and ^{13}CO in the IR spectra of Fig. 5b, indicating that the gas-phase CO and adsorbed CO exchange with their isotopic counterparts at a rate much faster than the scanning rate of the IR. No other feature in the IR spectra changed during the course of the experiment, including those attributed to gaseous ethylene. The same conclusions can be drawn for all the spectra recorded during all the transient experiments.

Figure 6 shows the transient responses of ^{13}CO and $C_2H_5{}^{13}CHO$ during a pulse of ^{13}CO in the CO feed for CO partial pressures of 0.0083, 0.0167, and 0.0417 MPa. The partial pressures of hydrogen and ethylene were kept constant at 0.025 MPa each and helium was used as a diluent. The decrease in the residence time of ^{13}CO in each figure is due to increasing the CO flow rate (i.e., CO partial pressure) to flush the 10 cm^3 of ^{13}CO in the pulsing loop. The figure shows that increasing partial pressure of CO causes the response of $C_2H_5{}^{13}CHO$ to lag behind the ^{13}CO response further, indicating that increasing the CO partial pressure increases the residence time of intermediates leading to propionaldehyde. In contrast, the TOF of propionaldehyde formation decreases with increasing CO partial pressure.

Figure 7 shows how the responses of ^{13}CO and $C_2H_5{}^{13}CHO$ vary with H_2 and C_2H_4 partial pressures. The response of ^{13}CO did not vary in these experiments because the flow rate of CO was kept constant. Figure 7 shows that as the partial pressures of the H_2 and C_2H_4 increased, the residence time of intermediates leading to the formation of propionaldehyde decreased.

From the transient response, the average residence time of the ^{13}CO adsorbed on the catalyst surface can be obtained by (10)

$$\tau_{^{13}CO} = \int_0^\infty tE_{^{13}CO}(t)dt. \qquad [2]$$

Since the gaseous CO and adsorbed CO exchange rapidly (Fig. 5), the gaseous ^{13}CO response measured by mass spectrometry can be used as the response for the adsorbed ^{13}CO. The average residence time of all intermediate species leading to the formation of ^{13}C propionaldehyde from adsorbed ^{13}CO can then be expressed as

$$\tau_{C_2H_5{}^{13}CHO} = \int_0^\infty tE_{C_2H_5{}^{13}CO}(t)dt - \tau_{^{13}CO}. \qquad [3]$$

It has been recently shown (24) that a good estimate of

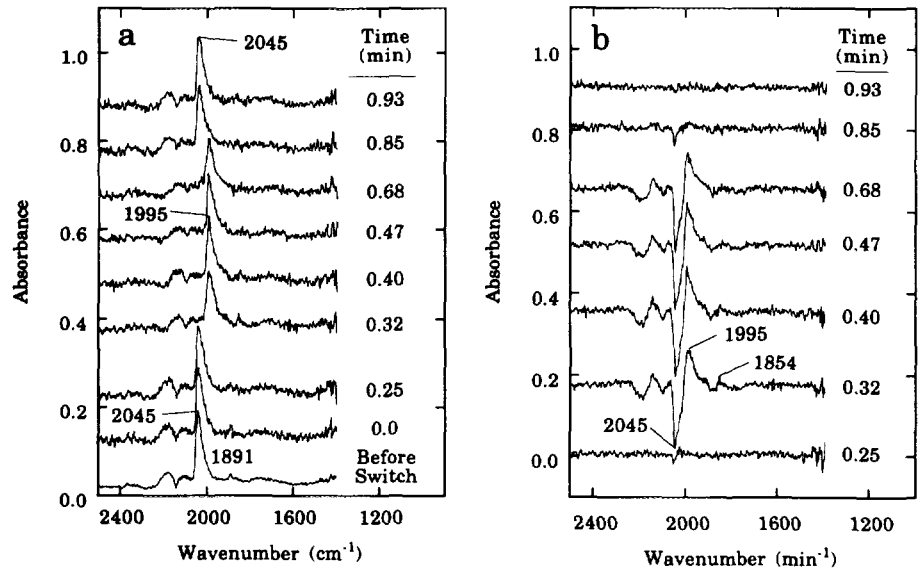

FIG. 5. (a) The *in situ* IR response to a pulse of ^{13}CO in the ^{12}CO feed. (b) The difference spectra during a pulse of ^{13}CO in the ^{12}CO feed.

the surface coverage of all intermediate species leading to the formation of propionaldehyde from adsorbed CO can be obtained by

$$\theta_{*C_2H_5CO} = \tau_{C_2H_5{}^{13}CHO} \cdot TOF_{C_2H_5CHO}. \quad [4]$$

The surface coverage is designated as $\theta_{*C_2H_5CO}$ for reasons discussed later.

Equations [2]–[4] were used to obtain $\theta_{*C_2H_5CO}$ from the transient responses of the ^{13}C-labeled gaseous CO and propionaldehyde at various partial pressures of reactants and the experimental results are shown as the symbols in Fig. 8. Figure 8 represents the adsorption isotherms of the intermediate species in propionaldehyde formation *during* the reaction. The surface coverage of intermediates shows a Langmuir isotherm-type dependence on CO and H_2 partial pressures under the conditions of the reaction. The surface coverage of intermediates exhibits a linear dependence on the partial pressure of C_2H_4 under these conditions. The relationship between the rate of formation of product species and the adsorption isotherms will be discussed after further analysis of the postulated catalytic mechanism.

DISCUSSION

Reaction Mechanism

The mechanism for heterogeneous hydroformylation has been postulated from its analogy with the homogeneous hydroformylation reaction (24, 25, 29, 31, 39). The generally accepted mechanism of the reaction is shown in Table 2 (24). The formation of propionaldehyde involves the partial hydrogenation of C_2H_4 to form an adsorbed ethyl species ($*C_2H_5$), insertion of adsorbed linear CO into the adsorbed ethyl species to form an adsorbed acyl species ($*C_2H_5CO$), and hydrogenation of the acyl species to produce propionaldehyde. Hydrogenation of the adsorbed ethyl species results in the formation of ethane. Based on the analogy between homogeneous and heterogeneous hydroformylation, the same type of surface adsorbed hydrogen and ethyl species is assumed to exist in both reactions (24). The rates of formation for methane and C_{3+} hydrocarbons are too small to be considered in the present study.

Kinetic Analysis

The empirical rate equations obtained from power-law expressions are usually sufficient for further modeling, design, and control of industrial catalytic reactors, but give limited insight into the reaction mechanism. The power law for the forward reaction is expressed in terms of the partial pressure of reactants, P_i,

$$\hat{TOF} = k \prod_{i=1}^{I} P_i^{\alpha_i} \quad [5]$$

where $\hat{TOF}$ is the estimated TOF from the kinetic model, k is the rate constant, i represents the individual reactants, and α_i is the rection order of each individual reactant. The parameters in Eq. [5], k and α_i, were fitted to the experimental data in Fig. 2 by a nonlinear least-squares approximation for both the TOF of propionaldehyde for-

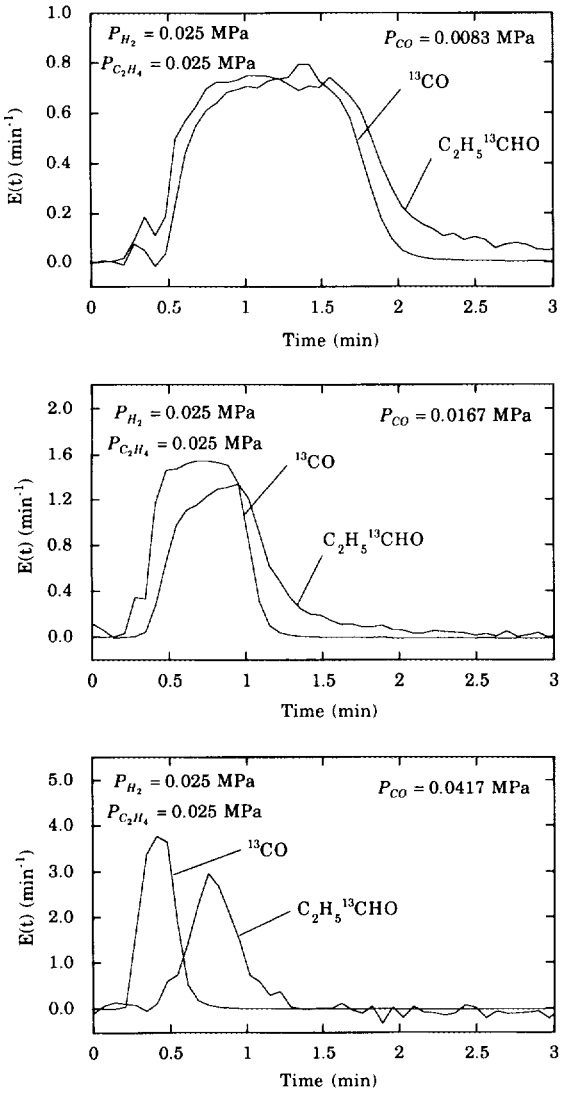

FIG. 6. The transient response of ^{13}CO and $C_2H_5{}^{13}CHO$ to a pulse of ^{13}CO in the ^{12}CO feed during ethylene hydroformylation for varying CO partial pressure.

mation and ethane formation using the MATHEMATICA software package. The results of the fit are shown in Table 3. The average percent error, $\Delta\%$, is used as a measure of the quality of the fit and is defined as

$$\Delta\% = \frac{100}{N}\sum_{n=1}^{N}\left|\frac{(\hat{\mathrm{TOF}}_n - \mathrm{TOF}_n)}{\mathrm{TOF}_n}\right|, \qquad [6]$$

where N is the number of experimental data points. From Table 3, the fit of the experimental data to the power law model yields an average of 11% error in propionaldehyde formation and a 4.9% average error in ethane formation. It must be noted that the fitting procedure for determining the reaction order for ethane formation is independent of the procedure for propionaldehyde formation. Both ethane and propionaldehyde power law models yield near first-order dependence on the partial pressures of both hydrogen and ethylene. Both power-law models are negative order under CO partial pressure. The reaction orders with respect to the partial pressures of the reactant are in good agreement with the reaction orders found for propylene hydroformylation on Rh–Na/SiO_2 (27) and Rh–Co/SiO_2 (28). Olefin hydroformylation on Rh–Y zeolite exhibited half order with respect to hydrogen partial pressure (26, 40). These equations are simple and give insight into the dependencies of the reaction rate on the partial pressures of the reactants, but limited insight into the reaction mechanism or the kinetics of the elementary steps.

The fundamental approach for kinetic analysis of a heterogeneous catalytic reaction involves the postulation of a rate-determining step and the formulation of an equation to express the rate in terms of the concentrations of the reaction intermediates in that step (1, 9, 10, 13). The

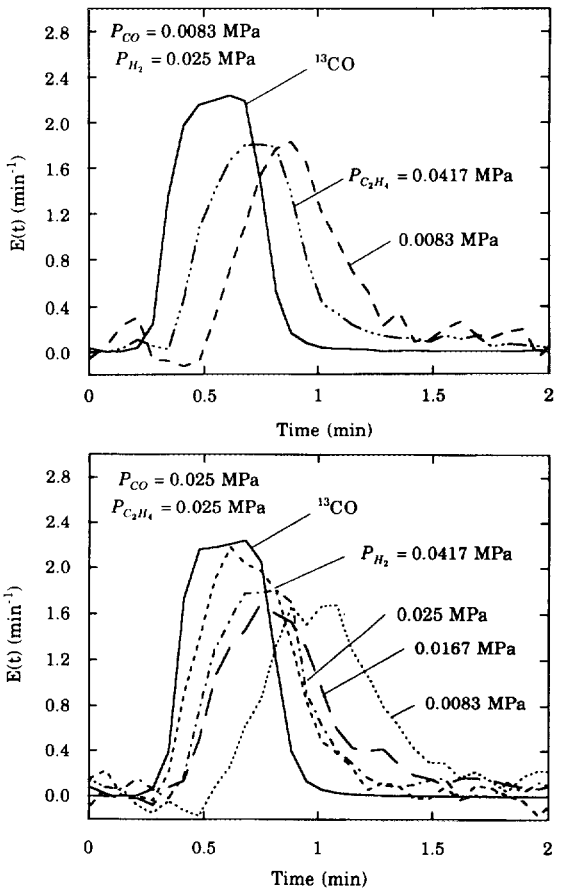

FIG. 7. The transient response of ^{13}CO and $C_2H_5{}^{13}CHO$ to a pulse of ^{13}CO in the ^{12}CO feed during ethylene hydroformylation for varying C_2H_4 and H_2 partial pressure.

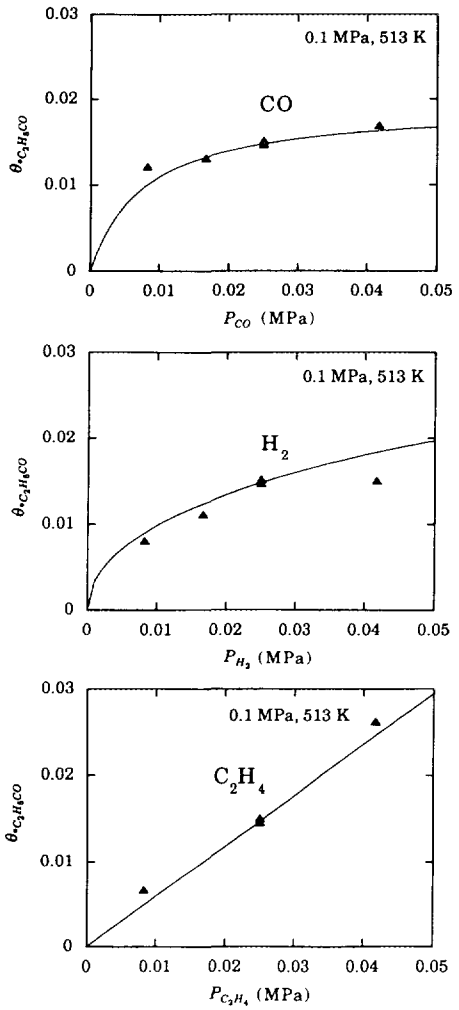

FIG. 8. Adsorption isotherms of $*C_2H_5CO$ as a function of partial pressures of reactants.

concentrations of the intermediates must then be related to the gas-phase concentration of the reactants and products (adsorption isotherms). The simplest theoretical expression for an adsorption isotherm is the Langmuir isotherm, on which the LHHW formalism is based. The underlying assumptions of the Langmuir isotherm include (9, 41): (i) monolayer coverage, (ii) uniformly energetic adsorption sites, and (iii) no interaction between adsorbed molecules. Assumption (i) is generally valid for heterogeneous catalysis. The structure-insensitive nature of hydroformylation makes assumption (ii) applicable to this study. Although surface interactions cannot be ignored, assumption (iii) is also considered in the LHHW formalism in this study to derive the rate laws for product formation and isotherm equations for adsorbates.

A rate-determining step (RDS) must be postulated for each product in the LHHW kinetic analysis. By comparing the proposed mechanism for both propionaldehyde and ethane formation in Table 2, elementary steps 1 through 4 cannot be considered as the RDS because they are common to both products. The use of these steps as RDS would lead to similar rate equations for both propionaldehyde and ethane formation. Step 7 is postulated as the only other alternative for the RDS of ethane formation. The RDS for propionaldehyde formation may be either steps 5, 6, or 8. Each RDS yields a different form of rate equation so that they can be distinguished from each other. The rate equation for propionaldehyde formation, assuming step 6 is the RDS, leads to the best fit of the data and will be derived and discussed here.

If we assume that the RDS for propionaldehyde formation is step 6, then the TOF for propionaldehyde formation can be expressed as

$$\hat{\mathrm{TOF}}_{C_2H_5CHO} = k_6\theta_{*C_2H_5CO}\theta_{*H}. \quad [7]$$

In conventional kinetic analysis θ is considered as an unmeasurable quantity and must be related to the measureable quantities such as the partial pressure of the reactants. By assuming that the other steps involved in propionaldehyde formation are in quasi-equilibrium, the surface coverage of *H, *CO, and $*C_2H_5CO$ can be expressed as

$$\theta_{*H} = \theta_*\sqrt{K_1P_{H_2}} \quad [8]$$

$$\theta_{*CO} = \theta_*K_2P_{CO} \quad [9]$$

$$\theta_{*C_2H_5CO} = \theta_*\sqrt{K_1}K_2K_3K_4K_5P_{CO}\sqrt{P_{H_2}}P_{C_2H_4}, \quad [10]$$

where θ_* is the fraction of unoccupied sites and is an unmeasurable quantity. A site balance yields θ_* as a function of the partial pressures of the reactants and is found to be

$$\theta_* = \frac{1}{\left(1 + K_2P_{CO} + \sqrt{K_1P_{H_2}} + K_3P_{C_2H_4} + \sqrt{K_1}K_3K_4\sqrt{P_{H_2}}P_{C_2H_4} + \sqrt{K_1}K_2K_3K_4K_5P_{CO}\sqrt{P_{H_2}}P_{C_2H_4}\right)}. \quad [11]$$

Assuming that the coverages of *CO, *H, and $*C_2H_4$ are much larger than $*C_2H_5$ and $*C_2H_5CO$, Eqs. [9]–[11] can be combined to obtain the adsorption isotherm for the acyl intermediate and adsorbed CO in terms of the partial pressures of the reactants

$$\theta_{*C_2H_5CO} = \frac{\sqrt{K_1}K_2K_3K_4K_5P_{CO}\sqrt{P_{H_2}}P_{C_2H_4}}{1 + K_2P_{CO} + \sqrt{K_1P_{H_2}} + K_3P_{C_2H_4}} \quad [12]$$

TABLE 2

The Proposed Mechanism for Heterogeneous Hydroformylation on Rh/SiO_2

(Step 1)	$H_{2(g)} + 2* \overset{K_1}{\rightleftharpoons} 2*H$	$r_1 = k_{+1}P_{H_2}\theta_*^2 - k_{-1}\theta_H^2$
(Step 2)	$CO_{(g)} + * \overset{K_2}{\rightleftharpoons} *CO$	$r_2 = k_{+2}P_{CO}\theta_* - k_{-2}\theta_{*CO}$
(Step 3)	$C_2H_{4(g)} + * \overset{K_3}{\rightleftharpoons} *C_2H_4$	$r_3 = k_{+3}P_{C_2H_4}\theta_* - k_{-3}\theta_{*C_2H_4}$
(Step 4)	$*C_2H_4 + * H \overset{K_4}{\rightleftharpoons} *C_2H_5 + *$	$r_4 = k_{+4}\theta_{*C_2H_4}\theta_{*H} - k_{-4}\theta_{*C_2H_5}\theta_*$
(Step 5)	$*C_2H_5 + *CO \overset{K_5}{\rightleftharpoons} *C_2H_5CO + *$	$r_5 = k_{+5}\theta_{*C_2H_5}\theta_{*CO} - k_{-5}\theta_{*C_2H_5CO}\theta_*$
(Step 6)	$*C_2H_5CO + *H \overset{k_6}{\rightleftharpoons} *C_2H_5CHO + *$	$r_6 = k_6\theta_{*C_2H_5CO}\theta_{*H}$
(Step 7)	$*C_2H_5 + *H \overset{k_7}{\rightleftharpoons} C_2H_{6(g)} + 2*$	$r_7 = k_7\theta_{*C_2H_5}\theta_{*H}$
(Step 8)	$*C_2H_5CHO \overset{k_8}{\rightleftharpoons} C_2H_5CHO_{(g)} + *$	$r_8 = k_8\theta_{*C_2H_5CHO}$

Note. K_i is the equilibrium adsorption parameter, $i = 1, 2, \ldots$; k_{+i} is the forward rate constant; k_{-i} is the backward rate constant.

$$\theta_{*CO} = \frac{K_2P_{CO}}{1 + K_2P_{CO} + \sqrt{K_1P_{H_2}} + K_3P_{C_2H_4}}. \quad [13]$$

$$T\hat{O}F_{C_2H_5CHO} = \frac{k_6K_1K_2K_3K_4K_5P_{CO}P_{H_2}P_{C_2H_4}}{(1 + K_2P_{CO} + \sqrt{K_1P_{H_2}} + K_3P_{C_2H_4})^2}. \quad [14]$$

The validity of the assumption will be further discussed. Equations [7], [8], and [12] can be combined to obtain

Similarly, the rate of ethane formation can be derived assuming step 7 is the rate-determining step

TABLE 3

Comparison of Different Kinetic Models

Kinetic model	Rate-determining step	Equations	Δ%
Power law	—	$TOF_{C_2H_5CHO} = 27.7P_{CO}^{-0.39}P_{H_2}^{0.90}P_{C_2H_4}^{1.15}$	11.0
		$TOF_{C_2H_6} = 6.05P_{CO}^{-1.30}P_{H_2}^{0.82}P_{C_2H_4}^{1.03}$	4.91
LHHW I	Step 5	$TOF_{C_2H_5CHO} = \frac{215000P_{CO}\sqrt{P_{H_2}}P_{C_2H_4}}{(1 + 639P_{CO} + 24.2\sqrt{P_{H_2}} + 0.000059P_{C_2H_4})^2}$	28.7
	Step 7	$TOF_{C_2H_6} = \frac{547000P_{H_2}P_{C_2H_4}}{(1 + 639P_{CO} + 24.2\sqrt{P_{H_2}} + 0.000059P_{C_2H_4})^2}$	6.51
LHHW II	Step 6	$TOF_{C_2H_5CHO} = \frac{444000P_{CO}P_{H_2}P_{C_2H_4}}{(1 + 322P_{CO} + 9.10\sqrt{P_{H_2}} + 0.0263P_{C_2H_4})^2}$	11.3
	Step 7	$TOF_{C_2H_6} = \frac{139000P_{H_2}P_{C_2H_4}}{(1 + 322P_{CO} + 9.10\sqrt{P_{H_2}} + 0.0263P_{C_2H_4})^2}$	6.55
LHHW III	Step 8	$TOF_{C_2H_5CHO} = \frac{101000P_{CO}P_{H_2}P_{C_2H_4}}{(1 + 749P_{CO} + 29.7\sqrt{P_{H_2}} + 0.0125P_{C_2H_4})}$	21.2
	Step 7	$TOF_{C_2H_6} = \frac{757000P_{H_2}P_{C_2H_4}}{(1 + 749P_{CO} + 29.7\sqrt{P_{H_2}} + 0.0125P_{C_2H_4})^2}$	6.33

$$\hat{\mathrm{TOF}}_{C_2H_6} = \frac{k_7 K_1 K_3 K_4 P_{H_2} P_{C_2H_4}}{(1 + K_2 P_{CO} + \sqrt{K_1 P_{H_2}} + K_3 P_{C_2H_4})^2}. \quad [15]$$

In this study, the variation of $\mathrm{TOF}_{C_2H_5CHO}$, $\mathrm{TOF}_{C_2H_6}$, $\theta_{*C_2H_5CO}$, and θ_{*CO} with the partial pressure of reactants are measured. Both overall kinetics (LHHW equations) and isotherm equations for adsorbed C_2H_5CHO and adsorbed CO derived from the proposed mechanism can be tested by comparison with the experimental results.

In contrast to the power law model, the TOF for both ethane and propionaldehyde formation depend on the same adsorption group in the denominator. For this reason, both Eqs. [14] and [15] must be taken into consideration simultaneously for estimation of the kinetic and adsorption parameters in the model. Using Baye's theorem, Box and Draper (42) derived a determinant minimization criterion in order to estimate unknown parameters in a multiresponse model with unknown variances and common parameters. For the present study, the criterion is to minimize

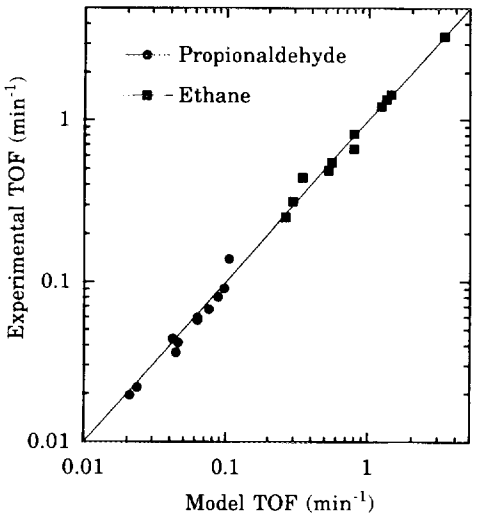

FIG. 9. Comparison of LHHW model for the reaction rate of ethane and propionaldehyde formation with experimental data during hydroformylation on Rh/SiO_2 at a total pressure of 0.1 MPa and 513 K.

$$c = \begin{vmatrix} \sum_{n=1}^{N} (\hat{\mathrm{TOF}}_{C_2H_5CHO} - \mathrm{TOF}_{C_2H_5CHO})^2 & \sum_{n=1}^{N} (\hat{\mathrm{TOF}}_{C_2H_5CHO} - \mathrm{TOF}_{C_2H_5CHO})(\hat{\mathrm{TOF}}_{C_2H_6} - \mathrm{TOF}_{C_2H_6}) \\ \sum_{n=1}^{N} (\hat{\mathrm{TOF}}_{C_2H_5CHO} - \mathrm{TOF}_{C_2H_5CHO})(\hat{\mathrm{TOF}}_{C_2H_6} - \mathrm{TOF}_{C_2H_6}) & \sum_{n=1}^{N} (\hat{\mathrm{TOF}}_{C_2H_6} - \mathrm{TOF}_{C_2H_6})^2 \end{vmatrix}. \quad [16]$$

Explicit values of the parameters K_4, K_5, k_6, and k_7 cannot be found from Eqs. [14] and [15] since they are lumped into the kinetic factor term. Equation [16] was minimized using the function minimization routine in the MATHEMATICA software package.

The derivation and equation fitting procedure described above were used to estimate the parameters in the LHHW I, II, and III kinetic models for postulating steps 5, 6, and 8 as the RDS for propionaldehyde formation, respectively. Table 3 summarizes the parameters and the average percent error for the LHHW kinetic models. The best fit of the data occurs when step 6 is considered as the RDS for propionaldehyde formation. The LHHW II model fit the experimental data as accurately as the power-law model with five parameters instead of eight. Figure 9 is a plot of the experimentally measured TOF vs the TOF calculated from the LHHW II model and shows a good fit for both ethane and propionaldehyde formation over a wide range of rates. The small value of K_3 indicates that the amount of adsorbed ethylene is insignificant compared to the amount of *CO and *H. This amount can be neglected in the donominator. The inability of the LHHW I model to fit the propionaldehyde data in this study stems from $\sqrt{P_{H_2}}$ in the numerator in the model which cannot describe the near first-order dependence on H_2 partial pressure. The LHHW III model is unable to fit the data well because the denominator is first-order and cannot take into account the negative order in CO partial pressure. The same form of rate equation for ethane formation is derived for all three models because the same RDS step for ethane formation is postulated for all three models; therefore the same degree of accuracy is achieved. Using the LHHW approach to the steady-state rate analysis without consideration of any other data, it is concluded that the RDS step for propionaldehyde formation is the hydrogenation of the acyl species and the RDS for ethane formation is the hydrogenation of the ethyl species.

Analysis of Adsorption Isotherms

The power-law model and the LHHW II model provide the same level of accuracy for fitting the overall kinetic data. The drawback of the power law model is the lack of insight into the reaction mechanism while the LHHW model provides indirect evidence to support a proposed mechanism with a RDS. A "correct" LHHW model would also provide a high confidence level for extrapolation of the model outside the experimental region.

To further test the LHHW II model, the isotherms of the adsorbed intermediates obtained during the reaction will be used to determine the goodness of fit to the isotherms (Eq. [12]) from the parameter estimate listed in

Table 3 for the LHHW II model. Further, the integrated area under the IR intensity of the linear CO band, which is proportional to the surface coverage of *CO, will be compared to the CO coverage obtained from Eq. [13]. If the LHHW II model can be successfully tested by two sets of independent data, i.e., TOF vs P_i and θ_i vs P_i data, the model is likely to be the correct one which may accurately describe the reaction.

By inspection of the mechanism in Table 2, the $*C_2H_5CO$ and $*C_2H_5CHO$ species are intermediates between the adsorbed *CO and the gaseous propionaldehyde product, e.g.,

$$*CO \overset{*C_2H_5}{\rightleftharpoons} *C_2H_5CO \overset{*H}{\rightarrow} *C_2H_5CHO \rightarrow C_2H_5CHO_{(g)}.$$

In the LHHW II model, it was assumed that the hydrogenation of the $*C_2H_5CO$ species is the RDS in propionaldehyde formation. This assumption suggests that the $*C_2H_5CHO$ species desorbs to form gaseous propionaldehyde as soon as it is formed. As a result, $\theta_{*C_2H_5CO} \gg \theta_{*C_2H_5CHO}$ and the surface coverage measured by the transient isotopic method is approximately equal to the surface coverage of the acyl intermediate, $\theta_{*C_2H_5CO}$. Lumping all the intermediates (for the formation of C_2H_5CHO from *CO) into one pool as $\theta_{*C_2H_5CO}$ can be further justified by an approximate first-order response for the $C_2H_5{}^{13}CHO$ to a pulse ^{13}CO input. All the $C_2H_5{}^{13}CHO$ responses in Figs. 6 and 7 can be approximated by a first-order response with $E_{13_{CO}}$ as the input function. The first-order response reflects the dynamics of a pool which resembles a CSTR in reaction engineering and a mixing tank in process control (10, 43). Therefore the surface coverage measured from transient tracing is assigned to $\theta_{*C_2H_5CO}$.

The adsorption isotherm of $\theta_{*C_2H_5CO}$ (Eq. [12]) during the reaction can be further simplified by neglecting K_3 since K_3 is insignificant in the adsorption group. The parameters in the adsorption group appearing in rate Eqs. [14] and [15] are the same as those for the isotherm of $\theta_{*C_2H_5CO}$ (Eq. [12]) and the estimated parameters from the LHHW II model in Table 3 are used to obtain

$$\theta_{*C_2H_5CO} = \frac{\sqrt{K_1}K_2K_3K_4K_5P_{CO}\sqrt{P_{H_2}}P_{C_2H_4}}{(1 + 321.8P_{CO} + 9.101\sqrt{P_{H_2}})}. \quad [17]$$

Using Eq. [17] to fit the measured isotherms by least-squares approximation, the parameter $\sqrt{K_1}K_2K_3K_4K_5$ is estimated to be 1562 $MPa^{-5/2}$ with $\Delta\% = 9.95\%$. The measured $\theta_{*C_2H_5CO}$ agrees well with the fitted isotherms, as can be seen in Fig. 8 where the solid line is Eq. [17] and the symbols are the measured $\theta_{*C_2H_5CO}$.

Another isotherm equation which can be tested by the experimental data is Eq. [13]. Including the estimated parameters and neglecting $K_3P_{C_2H_4}$, Eq. [13] can be written as

$$\theta_{*CO} = \frac{321.8P_{CO}}{(1 + 321.8P_{CO} + 9.101\sqrt{P_{H_2}})}. \quad [18]$$

Assuming that the integrated areas under the linear CO IR bands in Fig. 3 are proportional to the concentration of *CO on the surface, θ_{*CO} in Eq. [18] at a specified P_{CO} and P_{H_2} multiplied by a proportionality constant should fit the area under the linear CO band taken under the same partial pressure. It must be noted that the IR absorbance spectra were calculated using $\log_{10}$-based absorbance. The area under the linear CO band is defined as

$$a_{*CO} = \int_{1950}^{2065} A(\nu)d\nu, \quad [19]$$

where $A(\nu)$ is the IR absorbance and ν is the wavenumber. The interval between 1950 and 2065 cm^{-1} was used to minimize the contribution of gaseous CO bands and the small bridged CO band. Figure 10 shows the data points taken from area under the linear CO band and Eq. [18] (solid line) multiplied by a factor of 12.96 cm^{-1}. This value corresponds to an intergrated absorption coefficient of 5.22 cm/μmol. This value is less than that previously reported for linear CO on supported Rh by a factor of ~2.3 (44, 45). The difference in the calculated integrated absorption coefficient can be compounded from the measurement of the size of the catalyst disk, integrated absorbances, and the calculated amount of CO adsorbed from the LHHW II model. It must also be noted that the integrated absorption coefficient may vary with surface coverage (46).

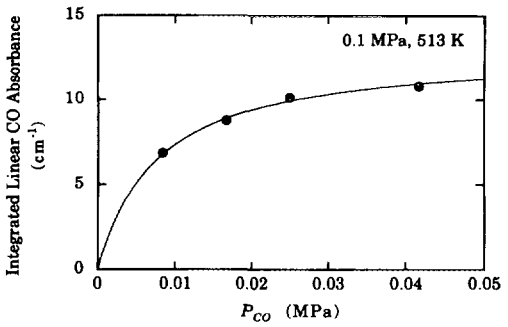

FIG. 10. Adsorption isotherms of *CO as a function of partial pressures of CO.

Figure 10 shows that Eq. [18], derived solely from the LHHW formalism, exhibits a remarkable fit to the integrated areas. The qualitative agreement between the measured θ_{*CO} and the θ_{*CO} calculated from Eq. [18] is further evidence that the LHHW II model describes not only the

overall rate but also the surface coverage of adsorbates in the ethylene hydroformylation reaction under the conditions of this study.

The values of the adsorption parameters in the model equations give insight into the surface coverages of adsorbed species during the reaction. The parameter K_2 is much larger than both K_1 and K_3, indicating that *CO is the most abundant surface species. The surface coverages of $*C_2H_4$, $*C_2H_5$, $*C_2H_5CO$, and $*C_2H_5CHO$ are insignificant in the site balance under the conditions of this study, as evidenced from the rate law of ethane and propionaldehyde formation and the adsorption isotherms depending mainly on P_{CO} and P_{H_2} in the denominator. The surface coverage of the $*C_2H_5CO$ was measured to be on the order of 0.007 to 0.026. This result also justifies the assumption of negligible surface coverage of this intermediate in the adsorption group of the LHHW II model.

The dominance of K_2, the adsorption equilibrium parameter for CO adsorption, may diminish the role of adsorbate interactions in the adsorption isotherm equations for the description of the dependence of surface coverage on reaction conditions. The lack of adsorbate interactions can also be seen from the invariance in the wavenumber of linear *CO with various partial pressures of hydrogen and ethylene in the IR spectra in Fig. 3. Due to the dominance of K_2 and the lack of pronounced adsorbate interactions, the assumption of no interaction between adsorbates appears to be valid for the derivation of the LHHW model for hydroformylation on the Rh/SiO_2 catalyst.

CONCLUSIONS

Four independent quantities, $TOF_{C_2H_5CHO}$, $TOF_{C_2H_6}$, $\theta_{C_2H_5CO}$, and θ_{*CO}, were measured as a function of partial pressure of reactants during steady-state ethylene hydroformylation over Rh/SiO_2. Pulsing ^{13}CO into CO flow shows that all the $C_2H_5{}^{13}CHO$ responses can be approximated by a first order response with $E_{^{13}CO}$ as the input function. The first-order response reveals that all the intermediates for the formation of $C_2H_5{}^{13}CHO$ from ^{13}CO can be lumped into one pool as adsorbed $C_2H_5{}^{13}CO$ of which coverage can be obtained from the average residence time of the $C_2H_5{}^{13}CHO$ response. θ_{*CO} was qualitatively determined from *in situ* IR spectroscopy.

Kinetic model (rate) equations for C_2H_5CHO and C_2H_6 formation and isotherm equations for adsorbed $*C_2H_5CO$ and *CO were derived using the LHHW approach from a proposed mechanism with ample support of experimental data. The proposed mechanism considers the hydrogenation of adsorbed $*C_2H_5CO$ as the rate-determining step for propionaldehyde formation and the hydrogenation of $*C_2H_5$ as the RDS for ethane formation. The LHHW model was tested by comparing the model rates and coverages with the measured rates of the product formation and coverage of adsorbates. The high degree of fitting of these equations suggests that the LHHW II model describes the surface reaction with high accuracy.

The results of this study demonstrate that the coverage of acyl intermediates determined from the dynamic response of an isotopic tracer is quantitatively consistent with that calculated from the LHHW formalism; the coverage of adsorbed *CO measured from IR spectroscopy is qualitatively consistent with that obtained from the LHHW formalism. Although the assumptions for the Langmuir isotherm do not account for interactions between adsorbates, the proposed mechanism and LHHW equations satisfactorily describe the kinetics, reaction pathway, and rate-determining steps for ethane and propionaldehyde formation. This study also shows that the measurement of coverage of adsorbates by both transient and IR techniques provides essential information to verify a proposed mechanism and kinetic model.

REFERENCES

1. Hougen, O. A., and Watson, K. M., *Ind. Eng. Chem.* **35,** 529 (1943).
2. Temkin, M. I., *Adv. Catal.* **28,** 173 (1979).
3. Smith, J. M., *Ind. Eng. Chem. Fundam.* **21,** 327 (1982).
4. Boudart, M., and Djeda-Mariadassou, G., "Kinetics of Heterogeneous Catalytic Reactions." Princeton Univ. Press, Princeton, NH, 1984.
5. Weller, S. W., *Catal. Rev. Sci. Eng.* **34**(3), 227 (1992).
6. Hougen, O. A., and Watson, K. M., "Chemical Process Principles Part III—Kinetics and Catalysis." Wiley, New York, 1947.
7. Tschernitz, J. L., Borstein, S., Beckmann, R. B., and Hougen, O. A., *Trans. AIChE* **42,** 883 (1946).
8. Hill, C. G., Jr., "An Introduction to Chemical Engineering Kinetics and Reactor Design." Wiley, New York, 1977.
9. Froment, G. F., and K. B. Bischoff, "Chemical Reactor Analysis and Design," 2nd ed. Wiley, New York, 1990.
10. Fogler, H. S., "Elements of Chemical Reaction Engineering," 2nd ed. Prentice–Hall, Englewood Cliffs, NJ, 1992.
11. Corma, A., Llopis, F., Monton, J. B., and Weller, S. W., *Chem. Eng. Sci.* **43,** 785 (1988).
12. Hutchinson, H. L., Barrick, P. L., and Brown, L. F., *AIChE Symp Ser.* No. 72, **63,** 18 (1967).
13. Satterfield, C. N., "Heterogeneous Catalysis in Industrial Practice," 2nd ed. McGraw–Hill, New York, 1991.
14. Weller, S. W., *AIChE J.* **2,** 59 (1956).
15. Kiperman, S. L., Kumbilieva, K. E., and Petrov, L. A., *Ind. Eng. Chem. Res.* **28,** 376 (1989).
16. Kiperman, S. L., *Chem. Eng. Commun.* **100,** 3 (1991).
17. Weller, S. W., *Adv. Chem. Ser.* **148,** 26 (1975).
18. Tamaru, K., *in* "Catalysis: Science and Technology" (J. R. Anderson and M. Boudart, Eds.), Vol. 9, p. 87. Springer-Verlag, Berlin/Hiedelberg/New York, 1991.
19. Boudart, M., *AIChE J.* **2,** 62 (1956).
20. Boudart, M., *Ind. Eng. Chem. Fundam.* **25,** 656 (1986).
21. Boudart, M., *Ind. Eng. Chem. Res.* **28,** 379 (1989).
22. Vannice, M. A., *J. Catal.* **37,** 462 (1975).
23. Lin, S. D., and Vannice, M. A., *J. Catal.* **143,** 563 (1993).
24. Balakos, M. W., and Chuang, S. S. C., *J. Catal.*, **151,** 253 (1995).
25. Chuang, S. C., and Pien, S. I., *J. Catal.* **135,** 618 (1992).

26. Takahashi, N., Matsuo, H., and Kobayashi, M., *J. Chem. Soc. Faraday Trans. 1* **80,** 629 (1984).
27. Natio, S., and Tanimoto, M., *J. Catal.* **130,** 106 (1991).
28. Reut, S. I., Kamalov, G. L., and Golodets, G. I., *Kinet Catal. Eng. Transl.* 694 (1991).
29. Chuang, S. S. C., Goodwin, J. G., and Wender, I., *J. Catal.* **92,** 416 (1985).
30. Chuang, S. S. C., Tian, Y. H., Goodwin, J. G., and Wender, I., *J. Catal.* **96,** 449 (1985).
31. Sachtler, W. M. H., and Ichikawa, M., *J. Phys. Chem.* **90,** 4752 (1986).
32. Jordan, D. S., and Bell, A. T., *J. Phys. Chem.* **90,** 4797 (1986).
33. Srinivas, G., Chuang, S. S. C., and Balakos, M. W., *AIChE J.* **39,** 530 (1993).
34. Sen, B., and Vannice, M. A., *J. Catal.* **113,** 52 (1988).
35. Somorjai, G., "Chemistry in Two Dimensions: Surfaces," p. 445. Cornell Univ. Press, Ithaca/London, 1981.
36. Cortright, R. D., Goddard, S. A., Rekoske, J. E., and Dumesic, J. A., *J. Catal.* **127,** 342 (1991).
37. Davis, M. E., Rode, E., Taylor, D., and Hanson, B. E., *J. Catal.* **86,** 67 (1984).
38. Hammaker, R. M., Francis, S. A., and Eichens, R. P., *Spectrochim. Acta.* **21,** 1295 (1965).
39. Chuang, S. C., and Pien, S. I., *J. Catal.* **128,** 596 (1991).
40. Rode, E. J., Davis, M. E., and Hanson, B. E., *J. Catal.* **96,** 563 (1985).
41. Langmuir, I., *J. Am. Chem. Soc.* **40,** 1361 (1918).
42. Box, G. E. P., Draper, N. R., *Biometrika* **52,** 355 (1965).
43. Stephanopoulos, G., "Chemical Process Control—An Introduction to Theory and Practice." Prentice-Hall, Englewood Cliffs, NJ, 1984.
44. Rasband, P. B., and Hecker, W. C., *J. Catal.* **139,** 551 (1993).
45. Duncan, T. M., Yates, J. T., Jr., and Vaughan, R. W., *J. Chem. Phys.* **73,** 975 (1980).
46. Winslow, P., and Bell., *J. Catal.* **86,** 158 (1984).